

934-27
2470
P-13

**SYNTHESIS AND CHARACTERIZATION OF ADVANCED
MATERIALS FOR NAVY APPLICATIONS**

J. Covino

**Naval Air Warfare Center Weapons Division
China Lake, CA. 93555-6001**

I. Lee

**Naval Air Warfare Center Weapons Division
China Lake, CA. 93555-6001**

ABSTRACT

The synthesis of ceramics and ceramic coatings through the sol-gel process has extensive application within the United States Navy and a broad range of potential commercial applications as well. This paper surveys seven specific applications for which the Navy is investigating these advanced materials. For each area, the synthetic process is described and the characteristics of the materials are discussed.

INTRODUCTION

The sol-gel process has been in use since 1950 [1]. However, it wasn't until the mid-1970s that increased interest by many researchers in this process became visible and the quantities of published papers, ranging from basic mechanistic understanding to applied component design, escalated. The sol-gel and modified sol-gel processes can be used to synthesize many advanced materials both for military and commercial applications. For example, the sol-gel process can be used for the manufacture of multicomponent glasses [2-5], coatings [6,7], fibers [8,9], monoliths [10,11], thermal insulation materials [12-14], controlled particle size powders [15,16], as well as special types of ceramics such as electronic ceramics [17,18], superionic conductors [19], and high-temperature super conductors [20,21].

This paper gives an overview of the synthesis, via the sol-gel process, of ceramics and ceramic coatings for use in specific Navy applications. Among the applications are coatings for electrochromic devices [22,23], laser gyro bodies [24-26], hermetic coatings for optical fibers for use in ocean environments [23,27], coating development for advanced lightweight structural applications [28-30], ceramic foams for catalysis and thermal insulation [31], and incorporation of organic and inorganic dyes in silica-based ceramics for lasers and ceramics for radomes [32-34]. The paper also addresses the characterization of these systems as well as advanced structural materials with respect to durability, chemical stability, optical properties, and other properties that are more specific to their applications and end use.

The sol-gel process is one in which the final product is obtained from reactive precursor materials (such as metal organics or metal alkoxides) by chemical or thermal means. This process involves the formation of a solution or colloidal suspension (sol) followed by a gelling stage (gel) prior to conversion to the final product. There are numerous advantages of sol-gel synthesis over the conventional melting techniques. Some advantages are (1) better homogeneity, (2) better purity, (3) speed and affordability, (4) lower temperature of preparation, (5) bypassing phase separations, (6) bypassing crystallization, (7) preparation of new noncrystalline solids outside the range of normal glass formation, (8) preparation of new crystalline phases from new crystalline solids, (9) better control of the fiber properties because it is easier to control gel properties than those of a melt, (10) better fiber products from special properties of the gel, (11) ability to be scaled-up for large production, (12) and tailorable microstructure and coating composition. When compared to the many advantages, the disadvantages are few: crack free non-porous coatings are difficult to manufacture, parts of the methodology are more of an art form than a well understood science, and purity can be difficult to control (i.e., carbon impurities are often measured).

The sol-gel process and the new materials that can be obtained by its use have tremendous commercial potential. Among these applications are the manufacture of high-quality oxide-based electronic substrates, coatings for use in the automotive industry, optical quality materials for a myriad of applications, high-temperature resistive coatings for use in industrial and consumer products, and controlled molecular sieves for use as catalysts and catalyst support in the petroleum and recycling industries.

EXPERIMENTAL

Synthesis

All oxides systems addressed in this paper were synthesized using the sol-gel process. The precursors used were high purity alkoxides, metal organics, or water-soluble salts. The specific syntheses and annealing processes used for each product can be found in the journal articles cited in each section.

Characterization

Characterization tools used to evaluate the chemical and physical properties of these materials included X-ray diffraction, thermal gravimetric analyses, thermal diffusivity, infrared spectroscopy, hydrogen permeation, electrochemical evaluation, scanning electron microscopy, dielectric properties measurements, and mechanical properties measurements. Not all techniques were used for all materials studied. For specific characterization and properties measured, refer to the references cited in each section.

RESULTS AND DISCUSSION

This section summarizes some of the pertinent material properties for each material studied. It does not give all the physical and chemical properties measured for each system. For more information on each class of compounds, refer to the proper references.

Coatings For Electrochromic Devices [22-23]

Electrochromism is the property of a material or system to change color reversibly in response to an applied potential. The use of ceramics in electronic applications is widespread and expanding rapidly (e.g., ECD displays and "smart windows"). For many of these increasingly demanding applications, improved materials and methods of fabrication are becoming necessary. The sol-gel process was used to synthesize a WO_3/Ni electrochromic device. This device was evaluated electrochemically in 0.3M LiClO_4 and $\text{NaClO}_4/\text{DMF}$ electrolyte solutions. Figure 1 shows the electrochemical results for the WO_3/Ni device in a 0.3m $\text{NaClO}_4/\text{DMF}$ electrolyte solution.

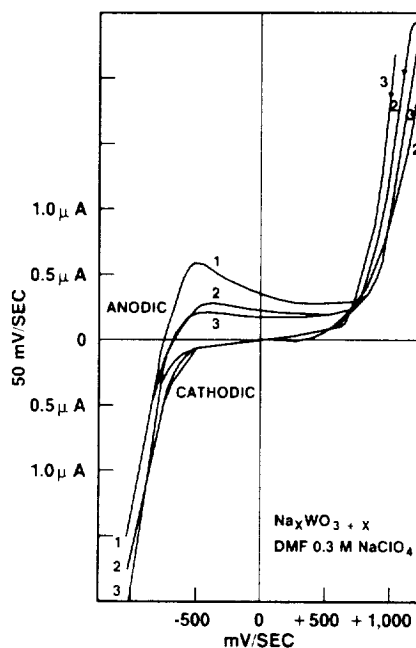


Figure 1. Electrochemical Cycling of the WO_3/Ni Device in a 0.3M $\text{NaClO}_4/\text{DMF}$ Solution With a Standard Calomel Electrode. A scan rate of 50 mV/sec was used.

Our major objective in this study was to demonstrate that the fine particulate nature of the sol-gel-deposited WO₃ could be stabilized in nonaqueous solvents, thus taking full advantage of the fast device response time engendered by small grain size and minimizing difficulties due to WO₃ dissolution. Layers of WO₃ coating formed on the nickel substrates were relatively thick (about 0.1 mm) and quite fragile. The particles produced by the sol-gel process were very small, and the WO₃ coating was nearly stoichiometric. Some dissolution of the WO₃ in DMF was noted. This was exacerbated in CH₃CN and DMSO; hence, only results obtained in DMF will be discussed here.

The electrochemical formation of the lithium bronze, Li_xWO₃, in nonaqueous media is a kinetically facile process at about -500mV (SCE). Formation of the Na_xWO₃ bronze occurs at significantly higher overpotentials (about -250 mV). The lithium bronze is stable, and reproducible cycling behavior is readily obtained. The sodium bronze appears to be less stable and less reproducible during cycling.

In both cases, the shift from the blue (bronze) to yellow (WO₃) state is readily achieved simply by stepping from -1,000 mV to +1,000mV. Unfortunately, response times are highly variable, depending not only on film thickness but also on the history of the electrode, the nature of the supporting electrolyte/intercalation cation, the cell geometry, and the solvent. The bronzes Na_xWO₃, for example, have colors ranging from golden yellow (x = 0.9) through red (x = 0.6) to deep violet (x = 0.3). These color changes are attributed to the oxidation state of tungsten, which is varying from VI to V, as well as to the molar ratio of the two concentrations.

Evidence of H⁺ inclusion in WO₃ overlays prepared by the sol-gel process has been observed using nonaqueous electrochemical studies. The H_xWO₃ phase is apparently readily converted (after a few cycles) to the Li_xWO₃ or Na_xWO₃ form. The irreversible formation of a more deeply blue-brown phase at high overpotentials was observed. The electrochromic devices presented in this study have been cycled reversibly for thousands of cycles.

Laser Gyro Bodies [24-26]

Lithium aluminum silicate (LAS) glass-ceramics have long been used in applications requiring ultra-low thermal expansion and in ultra-precision measurement experiments such as low helium gas permeability. However, for decades these glass ceramics have been made by conventional high temperature (above 1500°C) glass melting techniques. In order to demonstrate significant cost savings and improved material properties, the sol-gel process was explored in the synthesis of two glass ceramics. Table I summarizes these compositions.

Table I. Compositions of Nominal LAS Glass-Ceramic as Compared to Synthetic Sol-Gel-Derived NZ and NZP.

| Constituents | Nominal LAS | NZ | NZP |
|--|-------------|-------|-------|
| Silicon dioxide (SiO ₂) | 55.50 | 61.35 | 56.10 |
| Aluminum oxide (Al ₂ O ₃) | 25.30 | 27.97 | 25.60 |
| Lithium oxide (Li ₂ O) | 3.70 | 4.08 | 3.70 |
| Titanium dioxide (TiO ₂) | 2.30 | 2.30 | 2.30 |
| Magnesium oxide (MgO) | 1.00 | 1.00 | 1.00 |
| Zirconium dioxide (ZrO ₂) | 1.90 | 1.90 | 1.90 |
| Zinc oxide (ZnO) | 1.40 | 1.40 | 1.40 |
| Phosphorous pentoxide (P ₂ O ₅) | 7.90 | -- | 8.00 |
| Miscellaneous oxides (arsenic, iron, potassium, calcium, and sodium) | 1.01 | -- | --- |

Preliminary casting experiments were performed on NZ and NZP powders. Results showed that both NZ and NZP can be casted quite readily to produce a β-quartz lithium aluminum-silicate glass ceramic. Results of casting experiments (Figure 2) show that the most promising candidate was NZ-AH (produced by heating NZ at 2.93°C/min. to 735°C, holding for 6 hr.; heating at 2.17°C/min. to 800°C, holding for 96 hr.; cooling at 8°C/min.). This glass ceramic material exhibited an 82% crystallinity with crystallite size averaging 400Å. Both the virgilite and β-eucryptite structures are disordered quartz structures with varying degree of disorder. The NZ-AH material had a predominantly virgilite structure (or β-eucryptite structure, since the two X-ray powder patterns are very similar) and a 3-5% alpha-spodumene impurity. These results are in agreement with the currently most popular, commercially-available β-quartz LAS glass-ceramic material. By using the sol-gel process to make the LAS glass ceramics

significant reductions in annealing temperatures have been achieved, 800°C maximum with gelation and 1500 to 1700°C with conventional glass melting techniques.

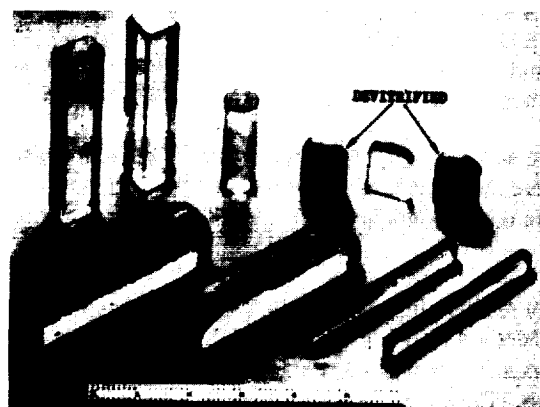


Figure 2. A Variety of Cast and Devitrified NZ Glass Samples.

Hermetic Coatings For Optical Fibers [23-27]

This section addresses a feasibility study to determine whether the sol-gel method could be employed for SiO₂ optical fiber coatings. Many fiber optical communication applications can be made possible with hermetically sealed coatings for SiO₂ fibers that are durable and nonpermeable to moisture, do not degrade the optical quality of the original fiber, and are cost effective and available. Materials of choice for the SiO₂ fiber coatings are LAS glass ceramics having stuffed β-quartz structure. These materials have crystalline phases from 60% to 100% and show low helium permeability. They have a low thermal expansion coefficient, with a varying from ±10⁻⁸ to 10⁻⁶ in the 0 to 600-K temperature range. They are very chemically and thermally stable, do not allow water to permeate, and have a composition of approximately 50% silica for material matching with SiO₂ fibers. It is because of these basic material properties that the LAS glass ceramic compositions are the materials of choice to attempt to make sol-gel coatings for SiO₂ fibers.

Two approaches were considered in the synthesis of these coatings. In Method I, a "LAS-like" composition chosen to be close to the nominal composition of a commercially available lithium aluminum silicate (CALAS) glass ceramic was prepared by the sol-gel method and was used as the coating material. In Method II, a finely ground CALAS composition was suspended into a tetra-ethoxysilane [TEOS, (C₂H₅O)₄Si] solution which was then used as the fiber coating. Table II shows the composition of the CALAS, with the weight percent of the representative oxides in it.

Table II. CALAS Composition Represented as Weight Percent of Oxide Present.

| Constituents | LAS (wt %) |
|--|------------|
| Silicon dioxide (SiO ₂) | 55.50 |
| Aluminum oxide (Al ₂ O ₃) | 25.30 |
| Lithium oxide (Li ₂ O) | 3.70 |
| Titanium dioxide (TiO ₂) | 2.30 |
| Magnesium oxide (MgO) | 1.00 |
| Zirconium oxide (ZrO ₂) | 1.90 |
| Zinc oxide (ZrO) | 1.40 |
| Phosphorous pentoxide (P ₂ O ₅) | 7.90 |
| Miscellaneous oxides ^a | 0.95 |
| Trace elements ^b | 0.01 |

^a Oxides of arsenic, iron, potassium, calcium, and sodium.

^b Trace elements such as barium, tin, manganese, lead, gallium, copper, silver, and strontium.

Two different sol-gel processes were used to make SiO₂ fiber optic coatings having the "LAS-like" compositions. X-ray diffraction data on dried powder made from the sol-gel Method I indicate that it is noncrystalline up to 800°C. Above 800°C, the powder appears to crystallize with a vergilite-like structure. It should also be noted that the currently most popular CALAS glass ceramic, which has the lowest helium permeability and thermal expansion coefficient, has an identical X-ray powder diffraction pattern. Thermal gravimetric analysis (TGA) data show that the majority of the solvent (water and alcohol) in the gel is removed by 80°C and thus makes such a treatment temperature adequate for heat treatment of the coated fibers.

From the optical microscope and scanning electron microscopy data, it was concluded that Method I produced better coatings. These coatings were better adhered to the SiO₂ fibers, and they were of a more uniform nature. Acid treatment of the SiO₂ fibers did make a pronounced difference in coating quality, with 49% HF showing the best results (see Figure 3).

In summary, the preliminary results illustrate that the coating adhesion and/or quality depends on (1) type and viscosity of the gel (Method I vs. Method II), (2) pretreatment of the SiO₂ fibers (no acid treatment vs. various types of acid treatment), (3) drying/annealing profile of the coated fibers (slower heating rates showed better coating adhesion), and (4) coating thickness. The sol-gel process offers the means to coat fibers by simple dipping techniques during production as well as to "fine tune" the chemical bonding of the coating to the fiber for strength and durability. It also offers a cost-effective and mass-production-suitable method to coat fibers during the drawing stages.



Figure 3. Scanning Electron Micrographs of Fibers Dipped in 49% HF Solution and Coated With Gel Synthesized Using Method I. Drying of the coatings was conducted at a rate of 0.5°C/min. to 80°C and held at 80°C for 6 hr.

Coatings for Light Weight Structural Applications [28-30]

Today there are many novel applications that require temperature resistant, lightweight, and durable coatings with properties far above presently available materials. Thus, much effort is going into the development and characterization of coatings. Coatings of choice are expected to be lightweight, have good mechanical properties, and show protection against oxygen and hydrogen both at cryogenic conditions and at high temperatures and pressures.

Protective coatings for both titanium-aluminum (Ti-Al) alloys and for carbon-carbon (C-C) composites have been synthesized and characterized with respect to protection against oxygen and hydrogen under both mild environments of low flows and low temperatures and severe environments of high flows and high temperatures. Mixed oxide glass ceramics were chosen as coating candidates because they are stable to temperatures of 1500°C, are nonreactive to oxygen, and are minimally reactive to hot hydrogen.

In the structural coatings effort three different synthetic methods have been addressed. These are: (1) the sol-gel process, the lacquer-slurry process, and the Chemical vapor deposition (CVD) method.

The sol-gel process for coatings is affordable and scalable. Coating composition can be tailored by the solution composition. Coating thickness and uniformity are controllable by solution viscosity, method and rate of coatings for application, and sintering conditions. In this work, the sol-gel method was used to develop coatings for Ti-al alloys. The Ti-Al alloys used were the α -2 Ti-Al and a variety of γ Ti-Al alloys. The coatings applied using the sol-gel method are Al₂O₃, Si-Al-oxide, and Si-Al-Ti-oxide.

The lacquer-slurry process involves the dispersion of powders into an organic lacquer, application of this slurry on the substrate, and sintering of the coated substrate to achieve densification. Coating composition can be controlled by both materials and lacquer selection.

The last type of coating application method investigated was the CVD method. SiC, Si₃N₄, ZrC, and Ni coatings were applied to C-C using the CVD method, and characterization of these coatings was performed. Table III summarizes the measured coating thickness for many of the coatings characterized in this study.

Table III. Measured Coating Thickness for a Variety of Coatings.

| Coating material/substrate | Method of application | Coating thickness |
|--|-----------------------|--------------------|
| Al ₂ O ₃ / α -2 Ti-Al | Sol-gel | 1.5 μ m |
| Si-Al-oxide/ α -2 and γ TiAl | Sol-gel | 1.5-6.0 μ m |
| C-C coatings | Lacquer slurry | 0.5 mm |
| SiC / C-C | CVD | 0.3 mm |
| Si ₃ N ₄ / C-C | CVD | 0.3 (0.17-0.59) mm |
| Ni / C-C | CVD | 0.3 mm |
| ZrC / C-C | CVD | 0.14 mm |

To evaluate Al₂O₃ and Si-Al-oxide coatings stability on both α -2 and γ Ti-Al alloy, Thermal gravimetric analyses were performed in oxygen and in hydrogen/inert gas (either Argon or Nitrogen). All TGA data were taken from room temperature to 1000°C at a rate of 2°C/min. Very little weight gain was observed for the Al₂O₃ coated α -2 Ti-Al alloy either in oxygen (1% weight gain) or in 10% H₂/90% N₂ (0.6% weight gain). However, the data show a significant increase in the rate of weight gain from 600 to 1000°C. Furthermore, when the coated α -2 Ti-Al alloy was removed from the TGA, coating flake-off was apparent. The TGAs show no signs of separation of the Al₂O₃ coating from the γ Ti-Al system and showed the coating to be more stable in both oxygen (0.6% weight gain) and 10%/H₂/90%N₂ (4% weight gain) than the coated α -2 Ti-Al alloy. The TGA residue for the Al₂O₃ showed no signs of separation from the γ Ti-Al alloy, this result is consistent with the γ Ti-Al being more oxygen resistant than α -2 Ti-Al.

The TGA data in Figure 4 clearly show that the coated α -2 Ti-Al alloy behaves better than the uncoated alloy in both pure oxygen and in 50% H₂/50% Ar (argon). In oxygen, the coated α -2 Ti-Al alloy gains less than 0.1 wt % as compared to a 6 to 10 wt % for the uncoated material. These data also show that the oxide coating significantly improves the reactivity of the α -2 Ti-Al alloy in 50% H₂/50% Ar. In hydrogen, the uncoated α -2 Ti-Al alloy gains 10 wt % and turns black, while the coated α -2 Ti-Al alloy gains only 0.6 wt % and has no apparent color change. It should be noted that both in oxygen and in 50% H₂/50% Ar, the coated material gains the majority of its weight by 300°C. After 500°C, the weight gain levels off. This study confirms that the Si-Al oxide coating is more thermally stable than the Al₂O₃ coating. For example, in the case of Si-Al-oxide coated α -2 in oxygen, a total weight gain of 0.1% was observed, while for the Al₂O₃ coated α -2 weight gain of 1% was seen.

Hydrogen permeation experiments were performed as a function of temperature (from 25°C to 300°C) using the "membrane permeation" technique. Data obtained for coated and uncoated C-C composites and for Si-Al-oxide coated and uncoated Ti-Al alloys are illustrated in Figures 5 and 6. These data were calculated by subtraction of the measured background level. When the sample achieved a desired temperature, it was saturated with deuterium for a 24-hr. period to assure equilibrium. To verify equilibrium, three flow rate measurements were made over an 8-hr. period. If the flow rate was equivalent all three times, the value was reported.

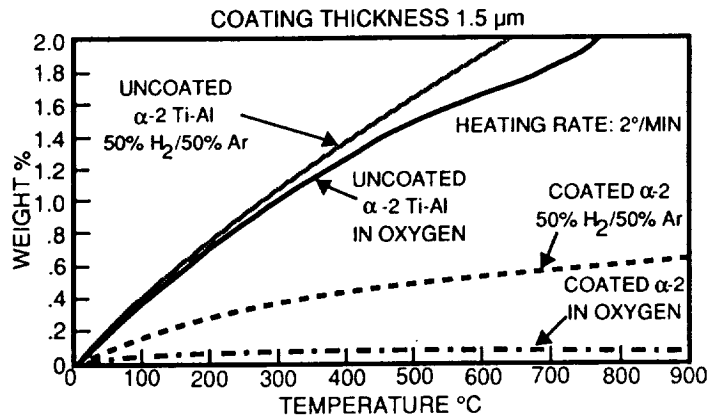


Figure 4. Thermal Gravimetric Analysis of Uncoated and Si-Al-Oxide Coated α -2 Ti-Al Alloy.

Figure 5. shows the permeability vs. temperature data for SiC, Si₃N₄, ZrC coated C-C composite, and uncoated C-C. The Figure key notes whether the C-C composite was coated on a single side or on both sides. The data show no temperature dependence, which is usually an indication that the samples have high porosity. The SiC (two sides) is the least hydrogen permeable coating for the C-C composites measured to date. The permeation data for ZrC-coated C-C composite illustrate that of the coatings evaluated, the ZrC coated by the CVD method tends to degrade the C-C substrate. The permeation data for ZrC coated C-C are higher than even the uncoated C-C composite. Further characterization of the ZrC C-C coating system is continuing in order to better identify changes that are taking place that can cause an increase the permeation with respect to uncoated C-C.

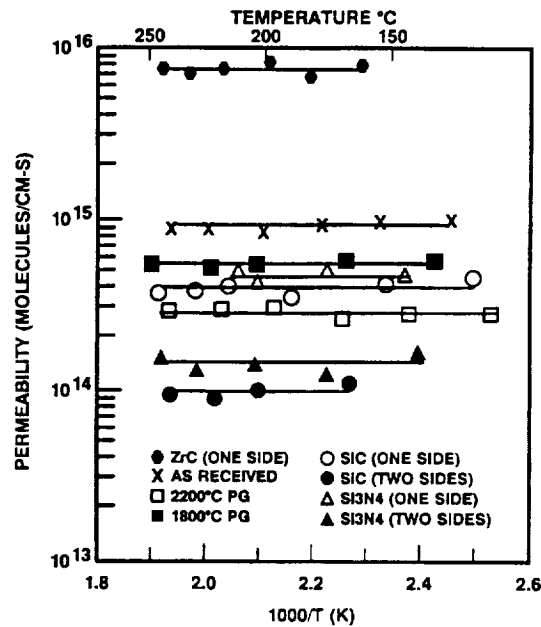


Figure 5. H₂ Permeability Vs. Temperature for Coated and Uncoated C-C Composites.

At low temperatures, the permeation of the Ni-coated C-C is 5×10^{10} molecules/cm-s, at approximately 200°C the permeation is 5×10^{10} molecules/cm-s; and at approximately 200°C the permeation is 2×10^{13} molecules/cm-s. The drastic increase in permeation at approximately 200°C was caused by spalling of the Ni coating. This conclusion was verified by post-test visual inspection.

Two Ti-Al alloys having nominal compositions of Ti-33Al-5Nb-1Ta (γ alloy) and Ti-14Al-20Nb-3.2V-2.0Mo (α -2 alloy) were coated with a Si-Al-oxide by the sol-gel process. The coated samples were annealed to 850°C before

any measurements were made. Hydrogen permeation measurements were performed on the coated and uncoated Ti-Al alloys, and the data are shown in Figure 6. The data show that the hydrogen permeability of the γ Ti-Al alloy is not very much affected by the 1.5 μm coating, while the permeability is drastically reduced for the coated α -2 Ti-Al alloy.

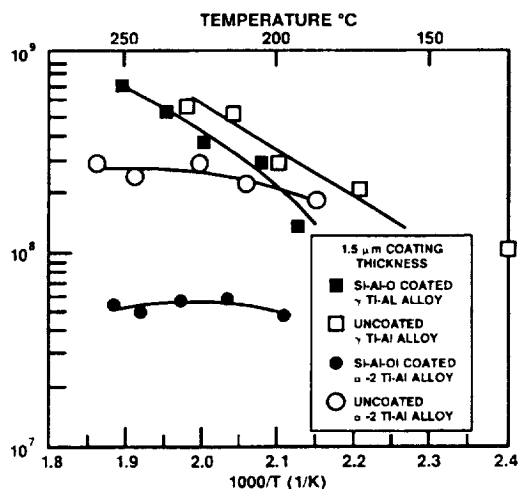


Figure 6. H_2 Permeability Vs. Temperature for Si-Al-Oxide Coated α -2 and γ Ti-Al alloys.

Ceramic Foams [31]

Today lightweight ceramics are finding many and varied applications due to their unique properties. These properties include high specific stiffness, high damping capacity, excellent dimensional stability, high thermal shock resistance, high surface area, low thermal conductivity, and low dielectric permittivity. This mix of properties makes the materials useful in either structural or functional applications such as high-temperature insulation, catalyst supports, chemical and moisture sensors, and as possible candidates for high-speed computer device packaging. Additionally, these porous materials offer a potential alternative for fabrication of composites by their infiltration with polymers, metals, fibers, or ceramics. Because of the ease of processing and their varied properties, these highly porous materials may lead to a new generation of lightweight ceramics and composites. Processing methods for cellular inorganic materials include foaming of molten glasses and cements, sintering of hollow glass spheres, and replication of polymer foams. Unfortunately, these processing methods are not reproducible, and materials with small, uniform cell size and with a tailored cell structure are very difficult to make.

Recently Fujii et al. [35] reported the use of a modified sol-gel process for making porous inorganic materials with tailored cell structure. The method applied the polymer foaming concept to sol-gel systems. Polymer foaming is performed by decomposition or evaporation of a foaming (Freon) agent followed by a rapid polymerization reaction to stabilize the foam structure. For this paper, the synthetic process of Fujii et al. [35] was used to synthesize SiO_2 ceramics having tailored cell structures for use as lightweight insulation materials. Characterization of these materials included: microstructure as a function of foaming process, density measurements, viscosity measurements as a function of time at different temperatures and varying pH, X-ray crystallography, dielectric constant measurements, and thermal diffusivity measurements.

A variety of cellular SiO_2 materials have been synthesized using a foaming sol-gel process and their properties have been characterized. The process uses the rapid viscosity change during gelation to stabilize the structure of a foamed silica sol. It was found that the properties of these porous oxides depend on the method of agitation and addition of Freon during the foaming process. However, in all samples, as the Freon concentration increased the percent porosity also increased and the density decreased. From 0 to 0.01 cc/g of Freon, the density ranged from 0.5 to 0.9 g/cc and the porosity ranged from 40 to 70%.

Dielectric constant measurements were also made on both sintered foams and incubated foams and are summarized in Table IV. The data show that the less dense samples have a lower dielectric constant when compared to the more dense samples.

Compression strength measurements on sintered cellular SiO₂ produced by the laboratory stirring process are shown in Table V. In all cases, except for the 0.005 cc/g of Freon samples, 10 to 20 samples were measured. The more dense samples are stronger (have a larger ultimate compressive strength). In the case of the 0.005 cc/g of Freon samples only two measurements were made, and the data is not accurate.

Table IV. Dielectric Constant for Cellular SiO₂ Taken at 10⁵ Hz.

| Type of SiO ₂ foams | Freon conc. (cc/g) | ε |
|--------------------------------|--------------------|------|
| Sintered foams | 0 | 1.72 |
| | 0.005 | 1.69 |
| | 0.01 | 1.52 |
| Incubated foams | 0 | 1.75 |
| | 0.005 | 1.63 |
| | 0.01 | 1.58 |

Table V. Ultimate Compressive Strength for Cellular SiO₂.

| Freon conc. (cc/g) | Ultimate compressive strength (psi) |
|--------------------|-------------------------------------|
| 0 | 487 ± 192 |
| 0.005 | 133 (two samples) |
| 0.01 | 251 ± 91 |

Thermal diffusivity data for sintered cellular SiO₂ are plotted in Figure 7. The scatter can be attributed to the irregular porosity of the samples. The data show a decrease in diffusivity with decreasing density.

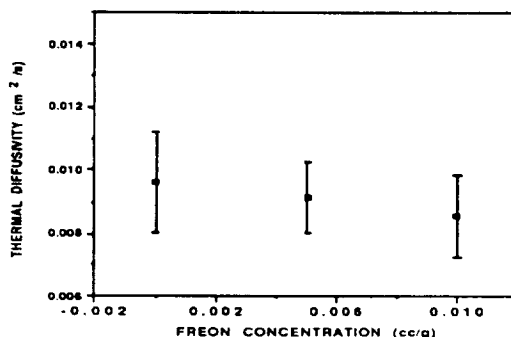


Figure 7. Thermal Diffusivity as a Function of Freon Concentration. Data taken at 25°C.

Incorporation Of Dyes In Silica Based Ceramics For Laser Applications [32-33]

In the past two decades, organic laser dyes have found wide use in different fields of science and technology including spectroscopy, optics, and lasers. The lasing media based on organic dyes may be in the form of solids, liquids, or gas. These lasing media cause spectral shifts of both absorption and emission and affect photochemical stability. They also alter the distribution between processes that the excited states may undergo. Although polymers are the earliest and the most common solid-state host for organic laser dyes, they have limited photostability and low thermal stability. Recently, sol-gel methods, with their low processing temperature, have made it possible to incorporate a dye into a transparent inorganic matrix. Embedding organic dyes into silica glass has significant advantages over the other types of matrixes. The silica glass is photochemically inert and can enhance the thermal stability of most organic dyes.

The sol-gel process was used to incorporate organic dyes including Rhodamine 6G (Rh6G), 2-(4-pyridyl)-5-(4-phenyl) oxazole (4PyPO) and the n-methyl tosylate salt of 2-(4-pyridyl)-5-(4-methoxy phenyl)oxazole (4PyMPO-MePTS) in silica gel. TGA and differential scanning calorimeter (DSC) analysis of the dye doped gels showed that the gel structure loses the adsorbed water molecules from room temperature to 150°C and decomposition of the dye molecules followed at the higher temperature. Absorption and emission of the dyes in the sol-gel glass matrix were also studied and compared with the results of the dyes in alcohol solution. The environments of the dye in silica were different than in alcohol solution.

TGA showed that all three of the dye-silica samples lost weight when heated to 600°C (Figure 8). This corresponds to a 20 to 25% weight loss. The approximately 5% weight loss below 150°C was due to the removal of physically adsorbed solvent molecules including surface water. The 15 to 20% weight loss up to ~600°C was due to the decomposition of residual organics and silanols. Above 600°C the weight loss was negligible. Figure 9 shows the DSC curves for the silica xerogels with and without the presence of dyes (the insertion is the DSC curve for 4PyMPO-MePTS itself). The curves indicate that the xerogels with dyes have a much broader exothermic peak between 250 and 350°C than silica itself, indicating that organic molecules are being oxidized. The figure also shows that silica gel has a much narrower endothermic peak at 150°C. In contrast, the silica samples that have the incorporated organic dye have much broader endothermic peaks. This result can be attributed to a combination of dye decomposition and silica dehydration.

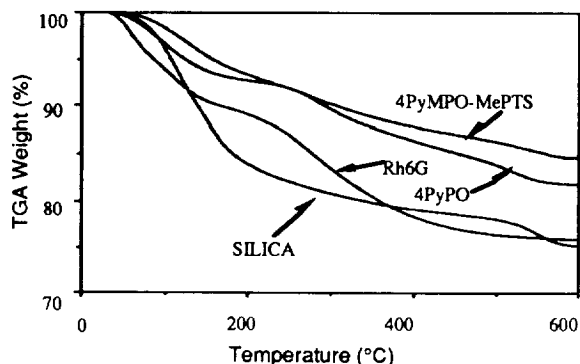


Figure 8. TGA Data for SiO₂ and SiO₂ With Incorporated Dyes.

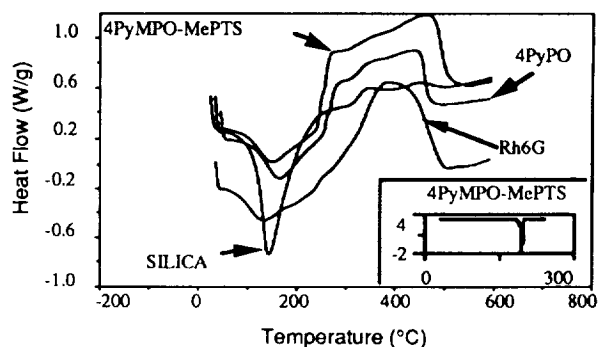


Figure 9. DSC Curves for Pure SiO₂ Gel and SiO₂ Gel With Incorporated Dyes.

Table VI summarizes the absorption and emission spectra of dyes in silica gel and solution. The experiments performed with Rh6G incorporated in silica gels have demonstrated that the silica matrix does not significantly alter the absorption maximum of the dye molecules when it is compared with the value in methanol. However, a slight blue shift (7 nm) in fluorescence spectra with respect to the methanol solution suggests that the silica gel is more polar, probably due to the remaining Me(OH)/H₂O solvent in the gel. Red shifts are observed for both absorption (6 nm) and emission (11 nm) spectra of 4PyMPO-MePTS in silica gel as compared with Et(OH)/H₂O solution. Since similar shifts are often observed in polar organic solvents [36], this may indicate that, in silica gel, the local environment around the dye is slightly less polar than an Et(OH)/H₂O solution.

Table VI. Emission and Excitation Characteristics of Rh6G, 4PyPO and 4PyMPO-MePTS in Silica Gel.

| Dye | In sol-gel silica matrix | | | In solution | |
|--------------|--------------------------|--------------------|----------------------------|--------------------------------|--------------------------------|
| | Fluorescence maximum | Absorption maximum | Fluorescence lifetime (rs) | Fluorescence maximum | Absorption maximum |
| Rh6G | 552 | 522 | 12.5 | 559 in Me(OH) | 523 in Me(OH) |
| 4PyPO | 493 | - | 12.5 | - | 325 in Et(OH) |
| 4PyMPO-MePTS | 568 | 408 | 10 | 562 in Et(OH)/H ₂ O | 397 in Et(OH)/H ₂ O |

For the 4PyPO dye, Ott et al. [37-38] reported that a significant spectral shift of absorption maxima in Et(OH)/HCl with respect to that in Et(OH) is due to the high reactivity of the nonbridging electrons on the pyridyl nitrogen atom for pyridine derivatives. Therefore, significant spectral shifts observed in silica gel compared to the solution spectra are due to the modification of dye chemistry in the initial sol and, subsequently into oxide gel.

Thermal analyzers (TGA and DSC) were used to study the thermal reaction of the gels with and without dyes. The TGA data indicated that the samples lost weight continuously until 600°C. The DSC data of the dye doped silica gel showed a broader endothermic peak than the silica gel itself, indicating the combination of silica dehydration and dye decomposition. Spectral shifts of the absorption and emission maxima to longer or shorter wavelengths were observed as compared to the dye solution spectra. This is attributed to a modification of the chemistry of the dyes with respect to their local environment during the incorporation of dye molecules into a liquid sol and, subsequently, into an oxide gel.

Ceramics for Radome Applications [34]

Ceramics based on monoclinic celsian ($\text{BaO} \cdot \text{Al}_2\text{O}_3 \cdot \text{SiO}_2$) can be useful in applications requiring high melting point, low thermal expansion, high thermal shock resistance, low dielectric constant and low $\tan \delta$, high frequency working capabilities, low and thermally stable dielectric constant, and low loss tangent. For example, celsian is a promising ceramic for use as a thermally stable dielectric and refractory material. Celsian has two polymorphs: the monoclinic and the hexagonal. The high-temperature polymorph, hexacelsian, undergoes a rapid and reversible transformation at 300°C from the hexagonal structure to an orthorhombic structure accompanying a significant volume change of approximately 3 to 4%. Therefore, this phase transformation in hexacelsian is detrimental in applications where the material is subjected to thermal cycling. Monoclinic celsian, on the other hand, does not undergo such a phase change. Unfortunately, hexacelsian readily forms during conventional solid-state processes at temperatures below 1590°C, and once this hexagonal structure is formed it is extremely difficult to transform to the desirable monoclinic phase. It would be desirable to provide a method for making pure monoclinic celsian at lower temperatures and shorter heating times without the use of contaminating additives.

Barium aluminosilicate (BAS) powders have been synthesized by the sol-gel process. X-ray analysis and thermal analysis including differential thermal analysis (DTA), DSC, and TGA, have been performed to characterize the powders. Also the effects of catalysts have been examined through an appropriate drying and sintering schedule for the formation of monoclinic celsian. It has been shown that the type of acid used as a catalyst controls the formation of polymorphs (hexagonal vs. monoclinic) of BAS ceramic. Because synthesis of monoclinic celsian by the sol-gel process requires relatively low temperatures and no seed crystals, it is less expensive, more manufacturable, and easier to scale up than other synthesis processes.

The scanning electron micrographs of the gels prepared from the sol-gel process using HCl, HF, and acetic acid catalysts of the hydrolysis process show significant morphological differences. The gels catalyzed with HCl and acetic acid appeared to be heterogeneous with rod-shaped barium salt that had crystallized during drying, while HF-catalyzed gel showed relatively good homogeneity with larger surface area.

Figure 10 shows composite curves of TGA and DTA data for the three samples. Although the total weight loss was dependent upon the method of synthesis, the average weight loss for all samples ranges from 20 to 30 wt % over the temperature range of 25 to 1000°C. It is interesting to notice that the gel catalyzed with HF undergoes BAS formation via a different mechanism than the gels catalyzed with HCl or acetic acid. The change in slope of the DTA baseline at 815°C in Figure 10(c) is indicative of a change in specific heat capacity, which corresponds to the gel-to-glass transition temperature. Around 1200°C, there is no significant weight change. Therefore, the broad exotherm shown in Figure 10(c) near this temperature was attributed to crystallization, and the endothermic peak at 1220°C is due to sample melting.

The X-ray pattern of BAS powder catalyzed with HCl and acetic acid show hexagonal phase formation even after extensive heat treatment. While the X-ray diffraction pattern for the gels catalyzed with HF showed the hexacelsian predominantly at low temperatures, the monoclinic phase dominated the X-ray powder pattern after annealing at 1200°C for many hours.

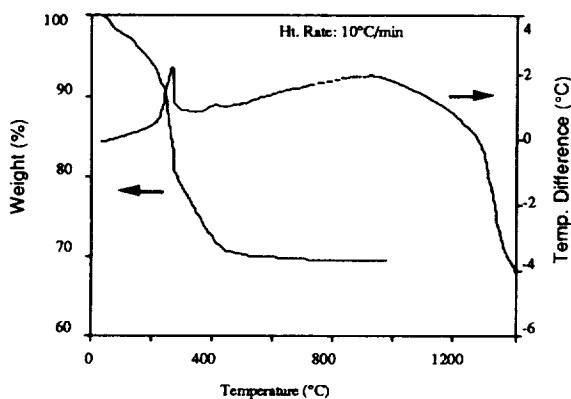


Figure 10(a). TGA and DTA Curves for the Gel Catalyzed With HCl.

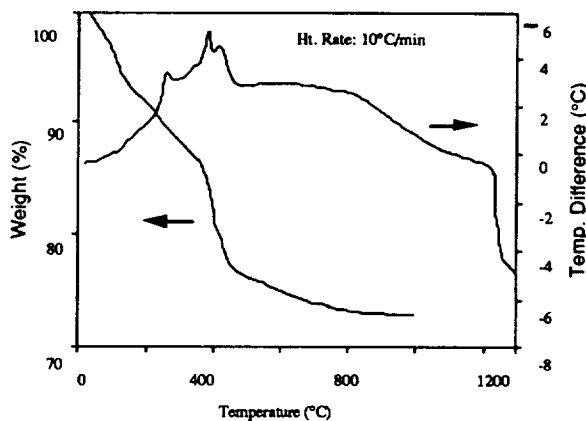


Figure 10(b). TGA and DTA Curves for the Gel Catalyzed With Acetic Acid.

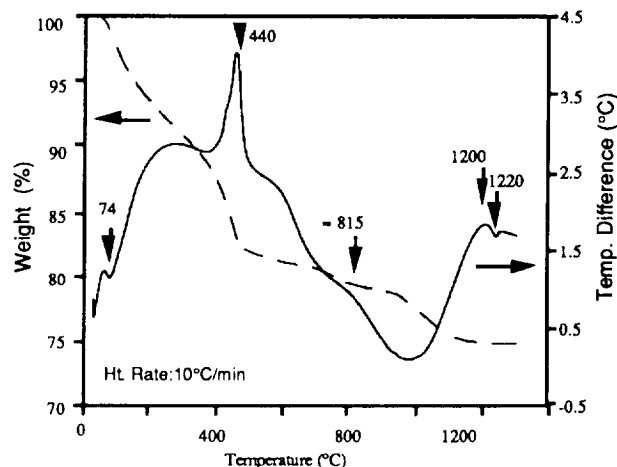


Figure 10(c). TGA and DTA Curves for the Gel Catalyzed With HF.

CONCLUSION

The sol-gel process offers great advantages for making films coatings, bulk ceramics, foams, and monoliths. This synthetic process offers control of microstructure and material properties during the entire process and can be commercialized quite readily due to the ease in scale up, versatility of materials, selectivity of properties, and low cost. The sol-gel process and the new materials that can be obtained by its use have tremendous commercial potential. Among potential commercial markets are electronics, automobiles, home insulation, toys, cosmetics, glass products, and consumer ceramics. This paper has presented only some examples of the materials that can be produced by the sol-gel process. The real commercialization of sol-gel derived materials can only be achieved if material scientists, chemists, and production engineers address the overall process and work together to remove possible obstacles.

REFERENCES

1. D. M. Ray and R. Roy, *Am. Mineralogist* 40, 1147 (1955).
2. M. Decottignies, J. Phalippou, and J. Zarzycki, *J. Mater. Sci.* 13, 2605 (1978).
3. S. J. Teichner, G. A. Nicolaon, M. A. Vicarini, and G. E. E Gardes, *Inorganic Oxide Aerogels, Advances in Coll, and Interface. Sci.* 5, 245 (1976).

4. I. M. Thomas, & J.J. Tillman, Ger. Offen. DE 3,247,1173, August 4, 1983; assigned to Owens-Illinois, Inc.
5. B. E. Yoldas, and T. W. O'Keeffe, *Appl. Opt.* 18, 3133 (1979).
6. C. J. Brinker, D. E. Clark, and D. R. Ulrich, Eds., *Mat. Res. Society Symposia Proceedings*, Vol. 32, NY: Elsevier Science Publishing Co. In., (1984).
7. L. C. Klein, Ed, *Sol-Gel Technology for Thin Films, Fibers, Preforms, Electronics and Speciality Shapes, Materials Sciences and Process Technology Series*, Noyes Publications, NJ, 1988, Part II. pp 50-136
8. W. C. La Course, Better Ceramics Through Chemistry. *Mat Res. Soc. Symp. Proc.* Vol. 32 (C. J. Brinker, D. E. Clark and D. R. Ulrich, Eds.), pp 53-58, North Holland, NY (1984).
9. W. Mahler, and M. F. Bechtold, *Nature* 285: 27-28 (1980).
10. L. C. Klein, Ed. *Sol-Gel Technology for Thin Films, Fibers, Preforms, Electronics and Speciality Shapes, Materials Sciences and Process Technology Series*, Noyes Publications, NJ, 1988, Part IV. 10, pp 200-222.
11. J. D. Mackenzie, in: *Ultrastructure Process of Ceramics, Glasses and Composites* (L. L. Hench and D. R. Ulrich, Ed), John Wiley and Sons, NY, 1984, pp 15-26
12. G. Dardel, S. Henning, and L. Svensson, European Patent Specification 0018 955 B 1, Date of Filing 17.4.1980, Date of Publication 1.12.1982.
13. P. H. Tewari, A. J. Hunt, and K. D. Lofftus, Advances in Production of Transparent Silica Aerogels, in: *Aerogels, Springer Proceedings in Physics 6*, J. Fricke (Ed.), Springer Verlag, Heidelberg, Berlin, New York, Tokyo (1986).
14. F. J. Broecker, W. Heckmann, F. Fischer, M. Mielke, J. Schroeder, and A. Stange, Structural Analysis of Granular Silica Aerogels, in: *Aerogels, Springer Proceedings in Physics 6*. J. Fricke (Ed.), Springer Verlag, Heidelberg, Berlin, New York, Tokyo (1986).
15. E. M. Rabinovich, *J. Non-Cryst. Solids*, 71, 1985, pp 187-193.
16. D. W. Johnson, Jr., *J. Amer. Ceram. Soc.*, 66, 1983, pp 683-688.
17. R. G. Dosch, *Mater. Res. Soc. Symp. Proceed.*, 32, 1984, pp 199-204.
18. K. Oda, and T. Yoshio, *J. Mater. Sci. Lett.*, 5, 1986, pp 545-548.
19. L. C. Klein, Ed., *Sol-Gel Technology for Thin Films, Fibers, Preforms, Electronics and Speciality Shapes, Materials Sciences and Process Technology Series*, Noyes Publications, NJ, Part V, Section 15, pp 303-329.
20. F. Uchikawa, H. Zheng, K. C. Chen, and J. D. Mackenzie, *Materials Research Society*, 1988, pp 89-92.
21. S. Kramer, G. Kordas, High-Temperature Superconductors II (Ed. D. W. Capone II, W. H. Butler (B. Batlogg, C. W. Chic) *Materials Research Society*, 1988, pp 67-68.
22. J. Covino and G. E. McMannis, *Material Research Society Symp. Proc.*, *Better Ceram. Chem.* 3, Vol. 121, pp. 553-556, 1988.
23. J. Covino and A.C. Finlinson, *5th Ultrastructure Processing of Ceramics, Glasses, Composites, Ordered Polymers and Advanced Optical Materials*, February 1991.
24. J. Covino, F. DeLaat, and R. Welsbie, *3rd International Workshop, "Glass and Glass Ceramics from Gels,"* Montpellier, France, 12-14 September 1985.
25. J. Covino, F. DeLaat, and R.A. Welsbie, *Mater. Res. Soc. Symp. Proc.*, Vol. 73, No. 2, *Better Ceram. Chem.*, pp. 135-142, 1986.
26. J. Covino, F. DeLaat, and R. Welsbie, *J. of Non-Cryst. Solids*, Vol. 82, No. 1-3, pp. 329-42, June 1986.
27. J. Covino and C. Wilson, *Third International Conference on Ultrastructure Processing of Ceramics, Glasses and Composites, Ultrastructure Processing of Advanced Ceramics*, pp. 981-993, John Wiley & Sons, Inc., 1988.
28. J. Covino and A. Finlinson, *1st international Symposium on Environmental Effects on Advanced Materials, ADVMAT/91* June 1991.
29. J. Covino, J. Dykema and A. Finlinson, *Minerals, Metals and Materials - High Performance Composites for the 1990's*, pp. 171-182, June 1990.
30. J. Covino, K. Klemm, and J. Dykema, *Mat. Res. Soc. Symp. Proc.* Vol. 175, pp 187-192.
31. J. Covino and A.P. Gehris Jr., *Material Research Society Symposium, Mech. Prop. Porous Cell. Mater.*, Vol. 207, pp. 129-134, 1991.
32. B. Abramoff, J. Covino, M.E. Hills and R. Chaundhuri, *Chemical Processing of Advanced Materials*, John Wiley & Sons, Inc., pp 973-979, 1992.
33. I. Lee, J. Covino, and M. Seltzer, *Better Ceramics through Chemistry V, Material Research Society Proc.* Vol 271, pp 657-661 (1992).
34. I. Lee and J. Covino, Sol-Gel Synthesis of Barium Aluminosilicate Ceramics, accepted for publication in the *Material Research Bulletin*, Sept. 1993.
35. T. Fujiu, G.L. Messing and W. Huebner, *J. Am. Ceram. Soc.* 73 (1), pg. 85 (1990).
36. D. Avnir, V.R. Kaufman and R. Reisfeld, *J. Non-Cryst. Solids*, 74, 395 (1985).
37. D.G. Ott, F.N. Hayes and V.N. Kerr, *J. Am. Chem. Soc.*, 78, 1941 (1956).
38. D.G. Ott, F. N. Haye, E. Hansbury and V.N. Kerr, *J. Am. Chem. Soc.*, 79, 5448 (1957).